PHYSICAL REVIEW B **81**, 100201(R) (2010)

Effective temperature in elastoplasticity of amorphous solids

Laurent Boué,[1] H. G. E. Hentschel,[2] Itamar Procaccia,[1] Ido Regev,[1] and Jacques Zylberg[1]
[1]*Department of Chemical Physics, The Weizmann Institute of Science, Rehovot 76100, Israel*
[2]*Department of Physics, Emory University, Atlanta, Georgia 30322, USA*
(Received 22 October 2009; revised manuscript received 16 January 2010; published 24 March 2010)

An effective temperature $T_{\rm eff}$ which differs from the bath temperature is believed to play an essential role in the theory of elastoplasticity of amorphous solids. Here, we introduce a natural definition of $T_{\rm eff}$ appearing naturally in a Boltzmann-like distribution of measurable structural features without recourse to any questionable assumption. The value of $T_{\rm eff}$ is connected, using theory and scaling concepts, to the flow stress and the mean energy that characterize the elastoplastic flow.

DOI: 10.1103/PhysRevB.81.100201 PACS number(s): 61.43.Fs, 81.05.Kf

Amorphous solids form when supercooled liquids are further cooled below the glass transition. While indistinguishable in their microscopic disorder from fluids, amorphous solids exhibit, in contradistinction from fluids, a yield stress below which they respond elastically to external strains; fluids flow under any external strain. Once the amorphous solid is subjected to large enough strains such that the response of the internal stress exceeds the yield stress, it can flow plastically in a manner that depends on the temperature, the shear rate, the density, etc. While there have been many attempts to present phenomenological equations to describe the rheology and the constitutive relations of such elastoplastic flows,[1–7] to this date none of these attempts have gained universal acceptance. In fact, there is no complete agreement even on the field variables or "order parameters" which are necessary to close a complete set of equations.

Among the more interesting ideas for order parameters stands the proposition that such elastoplastic flows exhibit two different temperatures: the regular temperature T that relates to the mean velocity of the particles forming the amorphous solid (and, naturally, to the heat bath to which the system is coupled) and an "effective temperature" $T_{\rm eff}$ that has to do with some "noise"[8] or "compositional properties" of the material.[9] The concept of effective temperature was originally formulated in Ref. 10 in order to describe the macroscopic properties of granular matter. Although these systems are athermal in the sense that they cannot evolve under normal temperature conditions, they may be driven by an external force which establishes an equilibrium-like behavior described by an effective temperature related to the intensity of the "tapping." These ideas have since been applied in other kinds of mechanically driven systems such as disordered elastic structures.[6,9,11–15] The aim of this Rapid Communication is to describe a simulational discovery of very sharp and direct meaning to an effective temperature in a number of simple computer models of elastoplasticity. This effective temperature has an obvious connection to the compositional disorder in the material. Moreover, it naturally identifies with the regular equilibrium temperature in the supercooled liquids. In this way it allows a smooth description that unites the supercooled regime with the amorphous-solid regime, something that is certainly lacking in many phenomenological descriptions. To define $T_{\rm eff}$ we need first to recall some recent advances in describing the supercooled equilibrium regime.

Upscaling in the supercooled regime. In a series of recent papers (cf. Ref. 16 and in particular Ref. 17) it was proposed that the scenario of the glass transition, including the astonishingly rapid slowing down of the dynamics in a short range of temperatures, is usefully encoded by the temperature dependence of the concentrations of a finite set of quasispecies which can be indexed by $1,2,\ldots,n$. The precise nature of these quasispecies may change from model to model, but they are always formed by particles and their nearest neighbors. The main advantage of these quasispecies is that they obey a discrete statistical mechanics, in the sense that their temperature-dependent concentrations $\langle C_i\rangle(T)$ are determined by a set of degeneracies g_i and enthalpies $\mathcal{H}_i$ such that

$$\langle C_i\rangle(T) = \frac{g_i e^{-\mathcal{H}_i/k_B T}}{\sum_{i=1}^{n} g_i e^{-\mathcal{H}_i/k_B T}}. \tag{1}$$

Obviously, if such a simple description is available, we can predict which quasispecies will be there when the temperature is high, and which will remain when the temperature decreases: only those with lowest free energy $\mathcal{F}_i \equiv \mathcal{H}_i - k_B T \ln g_i$ remain at low temperatures. Indeed, simulations show how the concentrations of some quasispecies decrease, some increase, and some start increasing and then decrease when temperature is lowered according to their degeneracy and enthalpy. Fluidity (or short relaxation times) is therefore correlated with high concentrations of quasispecies whose free energy is high, and solidity (or long relaxation times) is correlated with high concentrations of quasispecies whose free energy is low. This qualitative observation was made quantitative by noting the concentrations of those quasispecies that tend to disappear when the temperature is lowered and summing these concentrations to what was called the "liquid-like" concentration $\langle C_\ell\rangle(T)$. The inverse of this concentration provides a length scale (the typical distance between "fluid" quasispecies),

$$\xi(T) \equiv [\langle C_\ell\rangle(T)]^{-1/d}, \quad \xi \to \infty \text{ when } T \to 0, \tag{2}$$

where d is the space dimension. It was amply demonstrated on a large variety of models that the relaxation time $\tau_\alpha(T)$ measured using correlation functions in the supercooled regime is determined by this diverging scale according to

$$\tau_\alpha = \tau_0 e^{\mu\xi(T)/T}, \tag{3}$$

where μ is a typical free energy per particle and τ_0 is a microscopic (cage) time. In contradistinction with the Vogel-Fulcher and Adam-Gibbs fits, Eqs. (2) and (3) imply that there is no singularity associated with the glass transition at any temperature other than $T=0$, as was explained in Ref. 18. The simulational observation that we announce here is that the crucial statistical-mechanical relation (1) can remain correct and very useful, with T being replaced with $T_{\rm eff}$, also in the nonequilibrium elastoplastic regime of the amorphous solids that form at ultralow bath temperatures. In other words, $T_{\rm eff}$ exists for systems under strain and it determines the compositional disorder of the material.

Two models. We present the findings using two different models of glass formation in two dimensions: the first is the Shintani-Tanaka model[19] and the second is the so-called "hump model" which was inspired by Ref. 20 and analyzed in Ref. 17. The Shintani-Tanaka model has N identical particles of mass m; each of the particles carries a unit vector $\boldsymbol{u}_i$ that can rotate on the unit circle. The particles interact via the potential $U(r_{ij},\theta_i,\theta_j)=\bar{U}(r_{ij})+\Delta U(r_{ij},\theta_i,\theta_j)$. Here, $\bar{U}(r_{ij})$ is the standard isotropic Lennard-Jones 12-6 potential, whereas the anisotropic part $\Delta U(r_{ij},\theta_i,\theta_j)$ is chosen such as to favor local organization of the unit vectors in a fivefold symmetry to frustrate crystallization. For full details of this model the reader is referred to Refs. 19, 21, and 22; here it suffices to know that with the parameters chosen in Ref. 19 the model crystallizes upon cooling for $\Delta<0.6$, whereas for larger values of Δ the model exhibits all the standard features of the glass transition, including a spectacular slowing down of the decay of the correlation functions of the unit vectors $C_R(t)\equiv(1/N)\Sigma_i\langle \boldsymbol{u}_i(t)\cdot\boldsymbol{u}_i(0)\rangle$, which is very well described by Eq. (3).

The hump model again employs N identical particles interacting via a potential that is constructed as a piecewise function consisting of the repulsive part of a standard 12-6 Lennard-Jones potential connected at $r_0=2^{1/6}\sigma$ to a polynomial interaction $P(x)=\Sigma_i a_i x^i$. a_i's are tuned[17] so that $P(x)$ displays a peak at $r=r_{\rm hump}$ and also such that there is a smooth continuity (up to second derivatives) with the Lennard-Jones interaction at $U(r_0)=\epsilon h_0$ as well as with the cutoff interaction range $U(r_\star)=0$. The interaction potential for the hump model is shown in Fig. 1. Note that the two typical distances that are defined by this potential, i.e., the distance at the minimum $r_{\rm min}$ and the cutoff scale $r_\star$, appear explicitly in the amorphous arrangement of the particles in the supercooled liquid, as shown in the inset in Fig. 1. The model has two crystalline ground states: one at high pressure with a hexagonal lattice and a lattice constant of the order of $r_{\rm min}$. At low pressure the ground state is a more open structure in which the distance $r_\star$ appears periodically. At intermediate pressures the system fails to crystallize and forms a glass upon cooling.[17]

Simulations of the elastoplastic regime. The molecular-dynamics protocol we implemented for both models is the same. First, we carefully equilibrated a large number of independent configurations with N particles (N is varied in these simulations between 1024 and 6400) in the NVT ensemble using the Berendsen thermostat over a wide range of temperatures. These samples were then used to determine the enthalpies and degeneracies for the two models as described in detail in Ref. 17. These measured parameters predict accurately the concentrations of quasispecies at any given temperature as well as the τ_α relaxation time. After this, we turned our equilibrium supercooled liquids into amorphous solids by minimizing their potential energy (conjugate gradient algorithm), allowing us to sample a representative set of metastable minima. This procedure can be thought of as quenching a liquid infinitely fast into a disordered solid whose temperature is formally $T=0$. At this point we bring the particle velocities, using a short NVT run, to a value consistent with a desired bath temperature T_b. Then we force the system at a constant strain rate $\dot{\gamma}$ using the SLLOD algorithm combined with Lees-Edwards boundary conditions. Examples of typical stress-strain curves obtained for the hump model at different bath temperatures are shown in the lower left panel in Fig. 2. After the usual elastic response, an irreversible plastic flow begins, eventually generating a time-independent steady plastic flow in which all the thermodynamic quantities (such as the flow stress or energy) reached a value independent of the initial quenched configurations. The major finding is that throughout the evolution the concentrations of quasispecies obey Eq. (1) with the equilibrium measured values of g_i and $\mathcal{H}_i$, but with T_b being replaced with $T_{\rm eff}$, which is a function of T_b and $\dot{\gamma}$ (see, for example, the upper panels in Fig. 2). It is remarkable that there is an equally well-defined effective temperature not only in the steady state but also in the transient regime (see the lower right panel in Fig. 2). The steady-state values of $T_{\rm eff}$ as a function of T_b are shown for various values of $\dot{\gamma}$ in Fig. 3. Note that at high temperatures $T_{\rm eff}\to T_b$, whereas $T_{\rm eff}$ increases when $T_b\to 0$, increasing the fluidity of the system.

The relevance and importance of the steady-state effective temperature can be demonstrated by relating it to the mean energy and the flow stress, with the latter being the mean stress in the elastoplastic steady state. The mean energy per

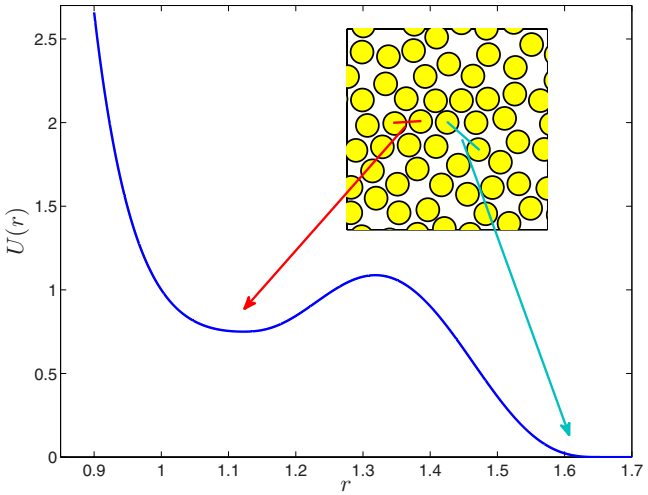

FIG. 1. (Color online) The pairwise potential for the hump model. In the inset we show a snapshot of the position of the point particles (the circles represent the finite range of interaction; cf. Ref. 17).

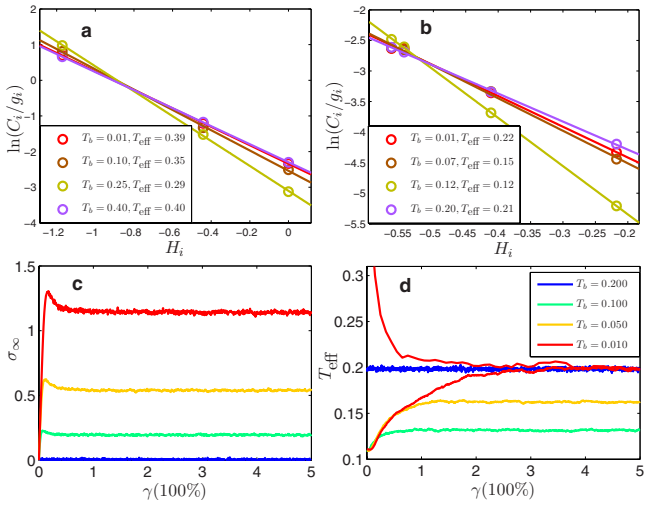

FIG. 2. (Color online) Upper panels: test of the Boltzmann-like distribution of the concentrations of quasispecies out of equilibrium using $T_{\rm eff}$ for the Shintani-Tanaka (left) and the hump (right) models. The degeneracies g_i and enthalpies $\mathcal{H}_i$ were taken from equilibrium simulations, but the concentrations C_i pertain here to elastoplastic steady states. Left lower panel: representative stress-strain curves for the hump model for different bath temperatures, color coded as in the right panel. Lower right panel: trajectories of $T_{\rm eff}$ for the hump model as a function time for a fixed strain rate $\dot\gamma = 10^{-4}$ and $N = 6400$, settling at the steady state either from above or from below.

particle U/N was directly measured in the steady state of the hump model and compared to the theoretical prediction

$$\frac{U}{N} = \frac{0.835}{2}\sum_i \langle C_i\rangle(T_{\rm eff})i + k_B T_b + \frac{\sigma_\infty^2(T_b)V}{2\mu N}, \qquad (4)$$

where the first two terms were taken from the equilibrium theory for the hump model in Ref. 17, but with $T_{\rm eff}$ replacing T_b in determining the concentrations of the quasispecies; the last term is the elastic energy per particle stored in the steady

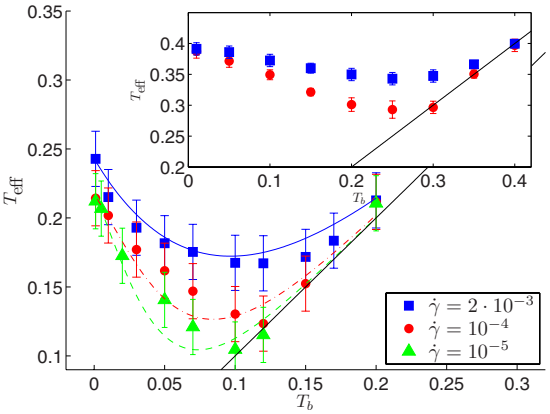

FIG. 3. (Color online) Symbols: $T_{\rm eff}$ as a function of T_b for the hump model at three values of the strain rate. Lines: prediction of $T_{\rm eff}$ using Eq. (5). Inset: $T_{\rm eff}$ as a function of T_b for the Shintani-Tanaka model at the two higher values of the strain rate. Straight lines indicate where $T_{\rm eff} = T_b$.

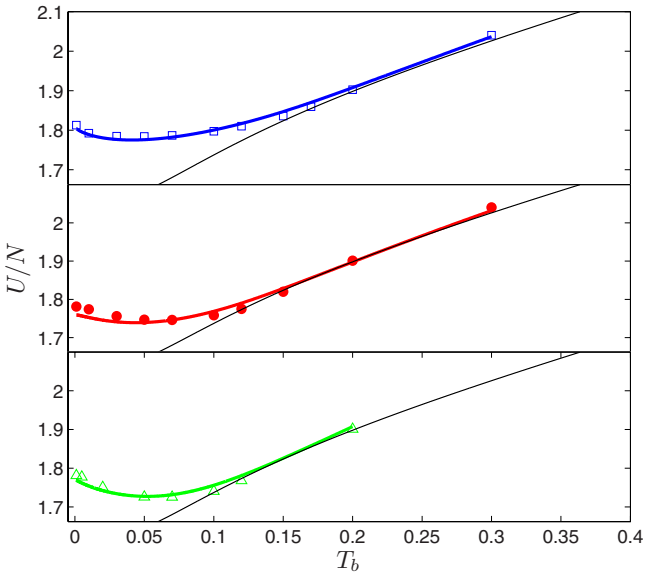

FIG. 4. (Color online) Energy per particle in the elastoplastic steady state as a function of the bath temperature. Symbols: simulation results. Lines through the symbols: theoretical prediction using Eq. (4). Black lines: equilibrium energy per particle.

state. The almost perfect agreement between the theoretical expectation based on $T_{\rm eff}$ and the direct measurement is demonstrated in Fig. 4.

The dependence of the flow stress on T_b for various values of $\dot\gamma$ is shown in Fig. 5. We show now that we can predict the values of the flow stress $\sigma_\infty(T_b, \dot\gamma)$ given the data for $T_{\rm eff}(T_b, \dot\gamma)$ or, vice versa, predict $T_{\rm eff}(T_b, \dot\gamma)$ from the knowledge of $\sigma_\infty(T_b, \dot\gamma)$. To this aim we invoke scaling concepts and propose a scaling form for $\sigma_\infty(T_b, T_{\rm eff})$ such that the $\dot\gamma$ dependence is carried here by $T_{\rm eff}$,

$$\sigma_\infty(T_b, T_{\rm eff}) = \frac{\rho}{m} k_B T_b f\left(\frac{T_{\rm eff}}{T_b}\right), \qquad (5)$$

where ρ and m are the density and the molecular weight of the particles. The function $f(x)$ is a dimensionless scaling

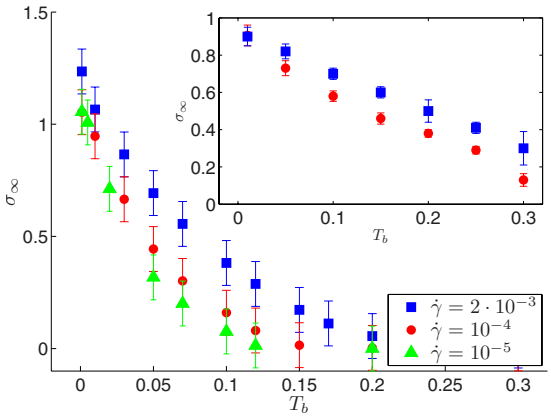

FIG. 5. (Color online) Flow stress as a function of T_b for the indicated values of the strain rate $\dot\gamma$ for the hump model, and in the inset for the Shintani-Tanaka model for the two higher values of the strain rate.

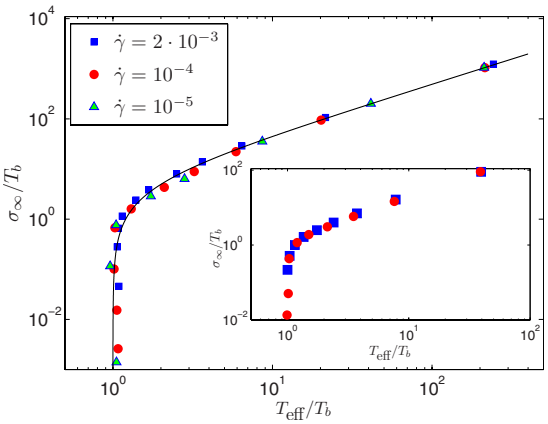

FIG. 6. (Color online) Double-logarithmic test of the scaling function (5); all of the data from Figs. 3 and 5 are replotted here for both models (with the Shintani-Tanaka model in the inset) to demonstrate the excellent data collapse. The continuous line is the function $f(x)=4.93(x-1)$.

function that must obey $f(1)=0$ to agree with the observed fact that at higher temperatures where $T_{\rm eff}=T_b$ the flow stress approaches zero. For $T\to 0$ or $x\to\infty$ we observed that σ_∞ becomes proportional to $T_{\rm eff}$ requiring $f(x)\to Cx$ for $x\to\infty$. The simplest function that obeys these limits is $f(x)=C(x-1)$. A test of the predicted data collapse is shown in Fig. 6 where the continuous line is the function $4.93(x-1)$. Having the scaling function at hand we can predict the data, say of $T_{\rm eff}(T_b,\dot{\gamma})$, from the knowledge of $\sigma_\infty(T_b,\dot{\gamma})$, or vice versa. Using for example the data for σ_∞ for the hump model in Fig. 5 and the scaling function $f(x)=4.93(x-1)$, we solve for $T_{\rm eff}(T_b,\dot{\gamma})$. The results are demonstrated in Fig. 3 with the curved lines going through the data. We conclude that the procedure is in satisfactory agreement with the data, demonstrating the importance of the concept of effective temperature. We mention in passing that the temperature T^* where $T_{\rm eff}$ separates from T_b can be easily predicted by equating the relaxation rate $\tau_\alpha(\xi(T))$ with $\dot{\gamma}^{-1}$: $T^*\sim\xi(T^*)\ \mu\ \ln\ \tau_0\dot{\gamma}$. At temperatures higher than T^* the natural relaxation time τ_α is the shorter of the two, whereas at temperatures lower than the minimum the shear rate determines the rate of relaxation.

Much remains to be done. For example, in the case of the standard model of binary mixtures we did not find a satisfactory upscaling that remains the same in and out of equilibrium. This and other riddles concerning the present approach will be dealt with in a future publication. Nevertheless, we believe that the present findings will provide grounds for future research.

This work was supported in part by the Israel Science Foundation and the German Israeli Foundation.

[1] A. S. Argon and H. Y. Kuo, Mater. Sci. Eng. **39**, 101 (1979).
[2] A. S. Argon, Acta Metall. **27**, 47 (1979).
[3] A. S. Argon and L. T. Shi, Philos. Mag. A **46**, 275 (1982).
[4] M. L. Falk and J. S. Langer, Phys. Rev. E **57**, 7192 (1998).
[5] P. Sollich, Phys. Rev. E **58**, 738 (1998).
[6] E. Bouchbinder, J. S. Langer, and I. Procaccia, Phys. Rev. E **75**, 036107 (2007); **75**, 036108 (2007).
[7] L. Bocquet, A. Colin, and A. Ajdari, Phys. Rev. Lett. **103**, 036001 (2009).
[8] P. Sollich, F. Lequeux, P. Hébraud, and M. E. Cates, Phys. Rev. Lett. **78**, 2020 (1997).
[9] E. Bouchbinder and J. S. Langer, Phys. Rev. E **80**, 031132 (2009).
[10] S. F. Edwards and R. B. S. Oakeshott, Physica A **157**, 1080 (1989).
[11] L. Cugliandolo, in *American Institute of Physics Conference Proceedings of the 1998 Buenos Aires Meeting*, edited by H. Falomir *et al.* (AIP, New York, 1998).
[12] L. Boué and E. Katzav, EPL **80**, 54002 (2007); S. Deboeuf, M. Adda-Bedia, and A. Boudaoud, *ibid.* **85**, 24002 (2009).
[13] L. Berthier and J.-L. Barrat, Phys. Rev. Lett. **89**, 095702 (2002).
[14] C. S. O'Hern, A. J. Liu, and S. R. Nagel, Phys. Rev. Lett. **93**, 165702 (2004).
[15] T. K. Haxton and A. J. Liu, Phys. Rev. Lett. **99**, 195701 (2007).
[16] E. Aharonov, E. Bouchbinder, V. Ilyin, N. Makedonska, I. Procaccia, and N. Schupper, EPL **77**, 56002 (2007); H. G. E. Hentschel, V. Ilyin, N. Makedonska, I. Procaccia, and N. Schupper, Phys. Rev. E **75**, 050404(R) (2007); E. Lerner and I. Procaccia, *ibid.* **78**, 020501(R) (2008); E. Lerner, I. Procaccia, and J. Zylberg, Phys. Rev. Lett. **102**, 125701 (2009); H. G. E. Hentschel, V. Ilyin, and I. Procaccia, *ibid.* **101**, 265701 (2008); H. G. E. Hentschel, V. Ilyin, I. Procaccia, and N. Schupper, Phys. Rev. E **78**, 061504 (2008).
[17] L. Boué, E. Lerner, I. Procaccia, and J. Zylberg, J. Stat. Mech.: Theory Exp. (2009), P11010.
[18] J. P. Eckmann and I. Procaccia, Phys. Rev. E **78**, 011503 (2008).
[19] H. Shintani and H. Tanaka, Nat. Phys. **2**, 200 (2006).
[20] M. Dzugutov, Phys. Rev. A **40**, 5434 (1989).
[21] V. Ilyin, E. Lerner, T.-S. Lo, and I. Procaccia, Phys. Rev. Lett. **99**, 135702 (2007).
[22] E. Lerner, I. Procaccia, and I. Regev, Phys. Rev. E **79**, 031501 (2009).